Pharmacological Research 207 (2024) 107346



Contents lists available at ScienceDirect

Pharmacological Research

journal homepage: www.elsevier.com/locate/yphrs





CD31 orchestrates metabolic regulation in autophagy pathways of rheumatoid arthritis

Kenneth CP Cheung [a,*,1], Jiao Ma [a], Lu Wang [a], Xingxuan Chen [a], Silvia Fanti [d], Mingzhang Li [e], Loiola Rodrigo Azevedo [c], Fabien Gosselet [c], Hao Shen [e], Xiaojiao Zheng [b], Aiping Lu [a,*], Wei Jia [b,f,**]

[a] Phenome Research Center, Hong Kong Baptist University School of Chinese Medicine, Hong Kong, China
[b] Center for Translational Medicine and Shanghai Key Laboratory of Diabetes Mellitus, Shanghai Sixth People's Hospital Affiliated to Shanghai Jiao Tong University School of Medicine, Shanghai 200233, China
[c] Faculté de Sciences Jean Perrin, Blood-brain barrier laboratory, Université d'Artois, France
[d] William Harvey Research Institute, Barts and The London School of Medicine and Dentistry, Queen Mary University of London, Charterhouse Square, London EC1M 6BQ, UK
[e] Department of Orthopaedics, Shanghai Sixth People's Hospital Affiliated to Shanghai Jiao Tong University School of Medicine, Shanghai 200233, China
[f] Department of Pharmacology and Pharmacy, The University of Hong Kong, Hong Kong, China

ARTICLE INFO

Keywords:
Endothelium
Rheumatoid arthritis
Inflammation
Autophagy
CD31
Glycolysis and oxidative phosphorylation

ABSTRACT

Synovitis is characterized by a distinctmetabolic profile featuring the accumulation of lactate, a byproduct of cellular metabolism within inflamed joints. This study reveals that the activation of the CD31 signal by lactate instigates a metabolic shift, specifically initiating endothelial cell autophagy. This adaptive process plays a pivotal role in fulfilling the augmented energy and biomolecule demands associated with the formation of new blood vessels in the synovium of Rheumatoid Arthritis (RA). Additionally, the amino acid substitutions in the CD31 cytoplasmic tail at the Y663F and Y686F sites of the immunoreceptor tyrosine-based inhibitory motifs (ITIM) alleviate RA. Mechanistically, this results in the downregulation of glycolysis and autophagy pathways. These findings significantly advance our understanding of potential therapeutic strategies for modulating these processes in synovitis and, potentially, other autoimmune diseases.

1. Introduction

Synovitis, characterized by inflammation of the synovial membrane lining the joints, plays a pivotal role in the pathogenesis of various rheumatic diseases. A critical aspect of synovial inflammation is the formation of new blood vessels, facilitating the influx of immune cells into the synovial membrane. Notably, the acidic environment of rheumatoid arthritis (RA) synovitis is partially attributed to the accumulation of lactate (LA) [1].

CD31 is a member of the immunoglobulin gene superfamily expressed prominently at high density at the lateral borders of endothelial cells (EC) [2]. The cytoplasmic tail of CD31 contains two immunoreceptor-tyrosine-based-inhibitory-motifs (ITIM), which, upon activation, selectively recruit src-homology 2 tyrosine phosphatases SHP-2 and SHP-1 [3,4]. Our recent research indicates that CD31-expressing ECs are highly activated and intricately involved in metabolic signaling in response to inflammatory stimuli, primarily through hemophilic interactions [3,4].

Autophagy, a fundamental pathway for degrading and recycling bioenergetic and biosynthetic components, responds to nutrient deprivation environments. Additionally, autophagy plays a pivotal role in modulating the response of ECs to various metabolic stressors, contributing to redox homeostasis and EC plasticity [5]. Despite its importance, the role of CD31 in autophagy remains unknown.

In this study, we delve into the response of CD31-expressing ECs to LA within the microenvironment of synovitis. Our investigation aims to identify key mechanistic steps in the cascade of events triggered by the response to LA in CD31 ECs, leading to metabolic switches and the

* Corresponding authors.
** Corresponding author at: Department of Pharmacology and Pharmacy, The University of Hong Kong, Hong Kong, China.
E-mail address: kcpcheung@hkbu.edu.hk (K.C. Cheung).
[1] lead contact

https://doi.org/10.1016/j.phrs.2024.107346
Received 30 April 2024; Received in revised form 18 July 2024; Accepted 7 August 2024
Available online 8 August 2024
1043-6618/© 2024 The Authors. Published by Elsevier Ltd. This is an open access article under the CC BY license (http://creativecommons.org/licenses/by/4.0/).

induction of autophagy.

2. Results

2.1. Elevated L-lactate, CD31, and associated autophagy expression in human RA

To investigate potential associations between LA, CD31, and autophagy in synovitis, two cohort studies were undertaken. In Cohort Study 1, LA concentration measured in synovial fluid was found to be elevated and correlated with increased progression in RA patients compared to healthy donors (Fig. 1A–B). Additionally, a positive correlation was observed between the number of CD31+ vessels and RA disease activity score(Fig. 1C).

Consistently, the immunohistological analysis demonstrated a significant increase in autophagy of CD31 in wild-type (WT) collagen-induced arthritis (CIA) mice, in comparison to CD31 knockout (KO) CIA mice. Mice treated with the CD31 ligation cross-linking antibody exhibited increased autophagy in the CIA model. In contrast, CD31 KO CIA mice exhibited a significantly elevated NADH dehydrogenase level (Supplementary Fig. 1A). These results collectively suggest that CD31 signalling plays an essential role in the RA autophagy and enzymatic reactions of energy metabolism.

2.2. CD31 signal is activated by lactate

In our immunoprecipitation studies, we observed that confluent CD31 WT ECs treated with L-LA triggers CD31 activation, leading to the recruitment of Src homology phosphatase 2 (SHP2), a known binding partner of CD31 signaling [3,4] (Fig. 2A-B). Subsequent validation through confocal and fluorescence-activated cell sorting (FACS) analyses demonstrated an upregulation of SHP2 recruitment in CD31 WT ECs treated with LA (Fig. 2C-F). We also observed that a higher Glut1 and HK2 expression in CD31 ECs (Fig. 2G, J).

To investigate whether LA-treated CD31 ECs might influence glycolysis, we treated both CD31 WT and KO ECs with 6-NBDG, a fluorescent glucose analog that accumulates in the cytoplasm, in the presence or absence of LA. We observed that a higher 6NBDG uptake in CD31 WT/ KO ECs with or without LA treatment for 6 h, quantified by flow cytometry (Fig. 2H–I**).** Additionally, we assessed the glycolytic capacity of both WT and CD31 KO ECs using the Seahorse assay to measure the extracellular acidification rate (ECAR), an indicator of glycolytic activity, revealing an increased ECAR in CD31 WT ECs treated with LA (Fig. 2K–L).

2.3. The CD31 signal mediates the nuclear translocation of STAT3

In WT CD31EC treated with LA, we observed an increased translocation of STAT3, a pivotal transcription factor implicated in RA progression, to the nucleus, indicating an upregulation of STAT3 activation (Fig. 2M). This observation was further substantiated by confocal analysis depicting the co-localization of STAT3 with DAPI within the nucleus of ECs treated with LA (Fig. 2N–O).

Subsequently, we conducted an examination of the transcription of mitochondrial tricarboxylic acid (TCA) cycle metabolites and genes in CD31 WT/KO ECs ± LA. Proteomic analysis revealed decrease in serine, threonine-protein kinase 3 in CD31 WT EC treated with LA. This kinase plays a significant role in cell growth and metabolism and its reduced presence suggest potential cellular stress and an adaptive increase in autophagy for energy generation and survival. Additionally, we observed a decrease in Cytochrome c oxidase subunit 5B, mitochondrial (COX5B), an essential component of the respiratory chain. This reduction implies possible mitochondrial dysfunction which could shift cellular metabolism towards glycolysis in WT ECs (Supplementary Fig.s S2A).

In CD31 KO ECs:LA, an increase in NADH dehydrogenase activity, suggesting enhanced mitochondrial respiratory chain function and upregulated oxidative phosphorylation. This enhancement may reduce these cells' reliance on autophagy compared to WT ECs:LA. Concurrently, levels of STAM-binding proteins were lowered, hinting at a potential decrease in cellular turnover and endocytosis-related activities (Supplementary Fig.s S2B).(Supplementary Fig.s S2B). KEGG pathway analysis indicated an association with an elevation in oxidative phosphorylation and mitochondrial respiration in KO:LA (Fig. S2C–D). Our findings aligned with FACS analysis of NADH dehydrogenase, cytochrome bc1 complex, and PKA levels (Fig. 3A–C) and western blot analysis (Fig. 3**D**). Additionally, we assessed the oxygen consumption rate (OCR), serving as an indicator of mitochondrial respiration, using Seahorse analysis. The maximal respiration was increased specifically in CD31 KO ECs treated with LA, but not in WT ECs treated with LA (Fig. 3E–F), suggesting that in the absence of CD31 signals, ECs engage mitochondrial respiration to meet energy demands. We therefore assessed mitochondria number and NADH in EC:LA. We further evaluated mitochondrial number and NADH levels in ECs treated with LA, revealing an increase in CD31 KO cells (Fig. 3G–H).

Intriguingly, in WT CD31 EC treated with LA, we observed induced autophagy, along with the accumulation and exocytosis of autophagosomes, as confirmed by transmission electron microscopy and flow cytometry (Fig. 3I–M).

2.4. CD31-induced EC autophagy

In elucidating the signaling pathway by which CD31 ECs contribute to autophagy promotion, we focused on AMPK and mTOR, the two major negative and positive regulators of autophagy, respectively. Our data reveals that CD31 WT ECs treated with LA exhibit an increase in AMPK phosphorylation but a decrease in mTOR activation (specifically mTOR phosphorylation at tyrosine 654) compared to CD31 KO ECs treated with LA (Fig. 4A–G).

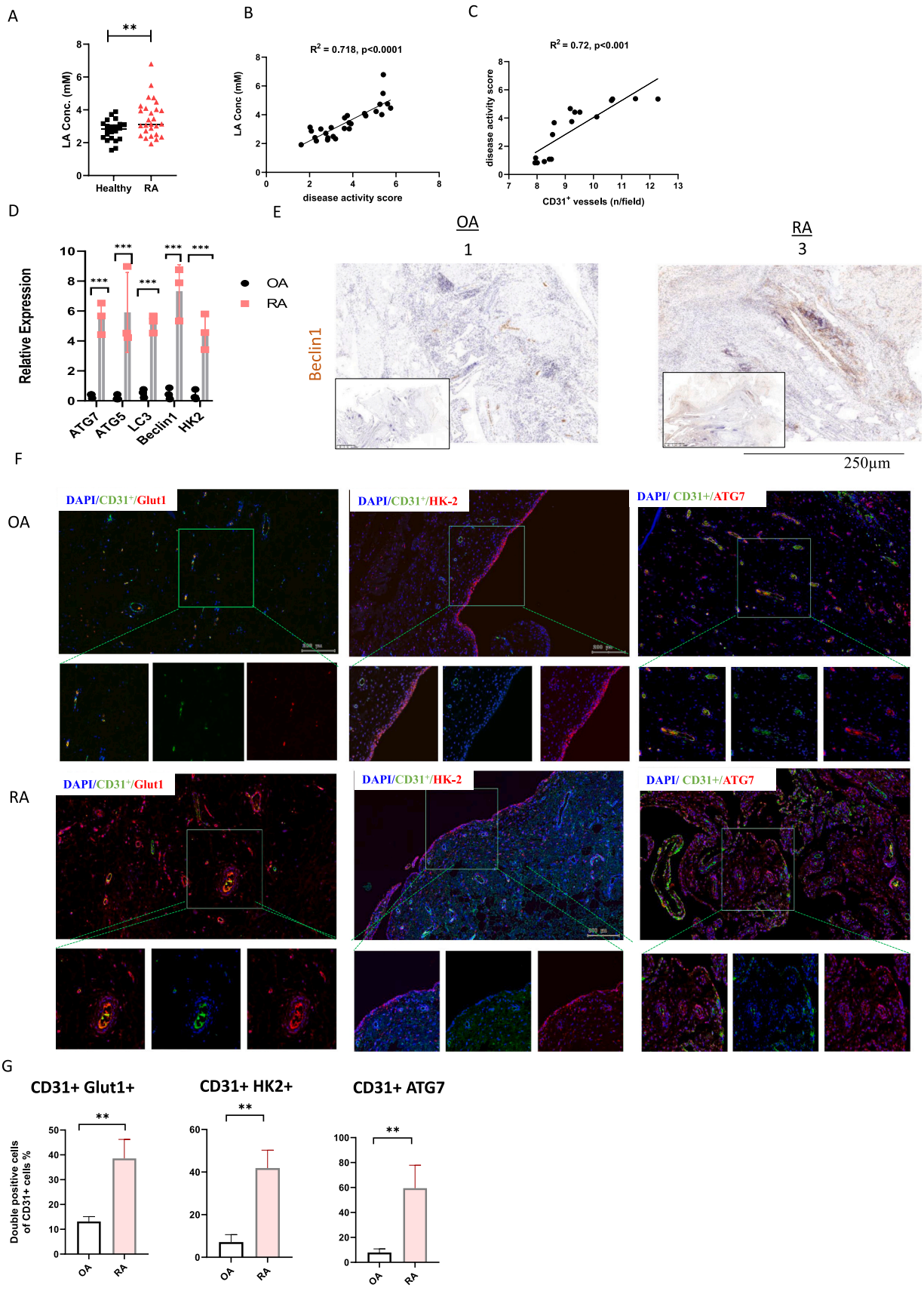
Further substantiating the requirement for endothelial metabolic adaptation in LA-rich conditions, treatment with 2-Deoxyglucose (2-DG, a glucose analog in which the hydroxyl group at the 2-position is replaced by a hydrogen atom) resulted in a reversal of the autophagy markers in CD31 WT ECs. However, this effect was not observed with etomoxir (Supplementary Fig. S3A-G), indicating the involvement of the glycolytic pathway in autophagy induced by CD31 WT [6]. Additionally, confocal analysis revealed increased hexokinase 2 (HK2) activation and decreased phosphorylated mTOR (p-mTOR) in CD31 WT ECs treated with LA, but not in KO (Supplementary Fig. S3H-J). These findings collectively confirm that CD31 promotes glycolysis in response to LA and activates autophagy.

2.5. CD31 regulates EC metabolites

Expanding upon these findings, we further identified potential signaling pathways that respond to biophysical changes induced by stress conditions, such as nutrient deprivation. We conducted primary cell measurements to examine alterations in fatty acids and amino acids. Notably, levels of succinic acid were significantly higher in WT EC treated with LA compared to KO EC treated with LA, while fumaric acid levels were decreased (Supplementary Fig. 4A). Furthermore, the fatty acid pathway exhibited modulation in WT EC compared to KO EC (Supplementary Fig. 4B–C). Additionally, the levels of various amino acids, including leucine, valine, tryptophan, phenylalanine, glutamine, and arginine, were reduced in WT EC treated with LA compared to KO ECs treated with LA (Supplementary Fig. 4D–E).

2.5.1. CD31 Y663F and Y686F mutations regulate autophagy and reduce the translocation of the STAT3 complex

Hypothesizing a causal connection between EC autophagy regulation by CD31, we sought to examine the histology of RA in mice with selective mutations of CD31 in the ITIM motif Y663 and Y686. For this



(caption on next page)

Fig. 1. Elevated LA, CD31 and associated autophagy expression in the synovial vasculature of human RA compared with OA. (A-B) Cohort Study 1, LA concentration was found to be elevated and correlated with increased progression in 27 RA patients (8 men, 19 women) compared to a group of 22 healthy donors (12 men, 10 women). The average ages for the two groups were 35.93±9.53 and 28.68±4.11 years old, respectively. (C) a positive correlation was observed between the presence of CD31+ vessels and disease activity scores. Cohort Study 2: This part of the study assessed CD31 and markers of autophagy within the synovial membrane. (D) Elevated mRNA levels of autophagy-related genes such as Beclin-1, ATG5, ATG7, and LC3, as well as the enzyme HK2, were detected in the synovial tissues of RA patients (5 females, average age 67.40±7.89 years) versus those with osteoarthritis (OA) (2 males, 4 females, average age 69.66±3.61 years). (E)Through immunohistochemistry, we observed a higher presence of Beclin-1 protein in RA patients compared to OA, with representative images showing the extent of Beclin-1 positive cells. The scoring for immunostaining ranged from 0 to 1 (<10 % positive cells) to 3 (51–80 % positive cells), with the scale bar representing 250 micrometers. (F) Detailed confocal microscopy showed a higher percentage of cells expressing CD31, Glut1, HK2, and ATG7 in RA synovial tissues compared to OA tissues. Analyses counted 500 cells per sample, with a scale bar of 200 micrometers (G) The results were depicted in bar charts. Data is presented as mean ± standard deviation. Statistical significance was determined using a two-tailed Student's t-test, with p-values less than 0.01 and 0.001 marked by ** and ***, respectively.

purpose, we used both constitutive (CRISPR/Cas9 technology [Y663F and Y686F]). We observed a decrease in RA severity as indicated by the H score in CD31 Y663F and Y686F CIA mice with decreased ATG7 expression. Conversely, we observed increased NADH levels in the RA-affected joints of Y663F and Y686F CIA mice (Supplementary Fig. S5). These findings suggest that the ITIM domain of CD31 is contributing to the regulation of autophagy and downregulate oxidative phosphorylation in our experimental model of CIA.

Similarly, CD31 gene constructs (CD31WT, CD31 pLKO.1, CD31 Y663F, and CD31 Y686F) were engineered and introduced into CD31 KO ECs through lentiviral transduction, as previously described [3]. Our findings show that CD31 Y663F, Y686F and pLKO.1 in ECs treated with LA resulted in a decrease expression of HK2 and 6NBDG uptake (Fig. 5A-E,H). Seahorse analysis further demonstrated that the Y663F, Y686F and pLKO.1 in the presence of LA decreased ECAR compared to WT EC (Fig. 5F–G). Additionally, CD31 Y663F, Y686F and pLKO.1 hindered AMPK phosphorylation, along with autophagy pathway inhibition in response to LA, confirming the central role of these motifs in autophagy regulation (Fig. 5I–K). Confocal analysis revealed that Y663F, Y686F and pLKO.1 downregulated HK2 and phosphorylated AMPK (pAMPK) (Fig. 6A–B). FACS analysis also indicated that, in comparison to WT CD31, Y663F,Y686F and pLKO.1 exhibited reduced levels pAMPK while pmTOR was concomitantly elevated (Fig. 6C–D). Importantly CD31 Y663F, Y686 F and pLKO.1 ECs treated with LA induced an elevation of the cytochrome bc1 complex and NADH dehydrogenase (Fig. 6E). As expected, these mutants upregulated mito-tracker accumulation and NADH, along with an increase in oxygen consumption rate (OCR) (Fig. 6F–I).

We subsequently analyzed STAT3 activation following LA-stimulation in both WT and mutant ECs. Western blot and confocal studies revealed that STAT3 was suppressed in LA- treated mutants and KO but not in WT ECs (Fig. 6J–L).

A schematic model illustrating CD31 metabolism via Y663 and Y686 and induced autophagy is summarized in the diagram (**Schematic diagram).**

3. Discussion

LA is a prominent by-product of cellular metabolism in inflamed tissues, particularly in chronic inflammatory conditions such as RA, where its accumulation triggers the inflammatory response. RA is characterized by three distinct histological patterns of synovitis, known as pathotypes [7]. Within the synovitis environment, there exists a highly adaptable metabolism that supports the cell growth and spread through various stages of synovitis. Moreover, the vasculature in RA is crucial for the movement and activity of immune cells, as it serves as the conduit for immune cell trafficking and facilitates the inflammatory response in the affected joints.

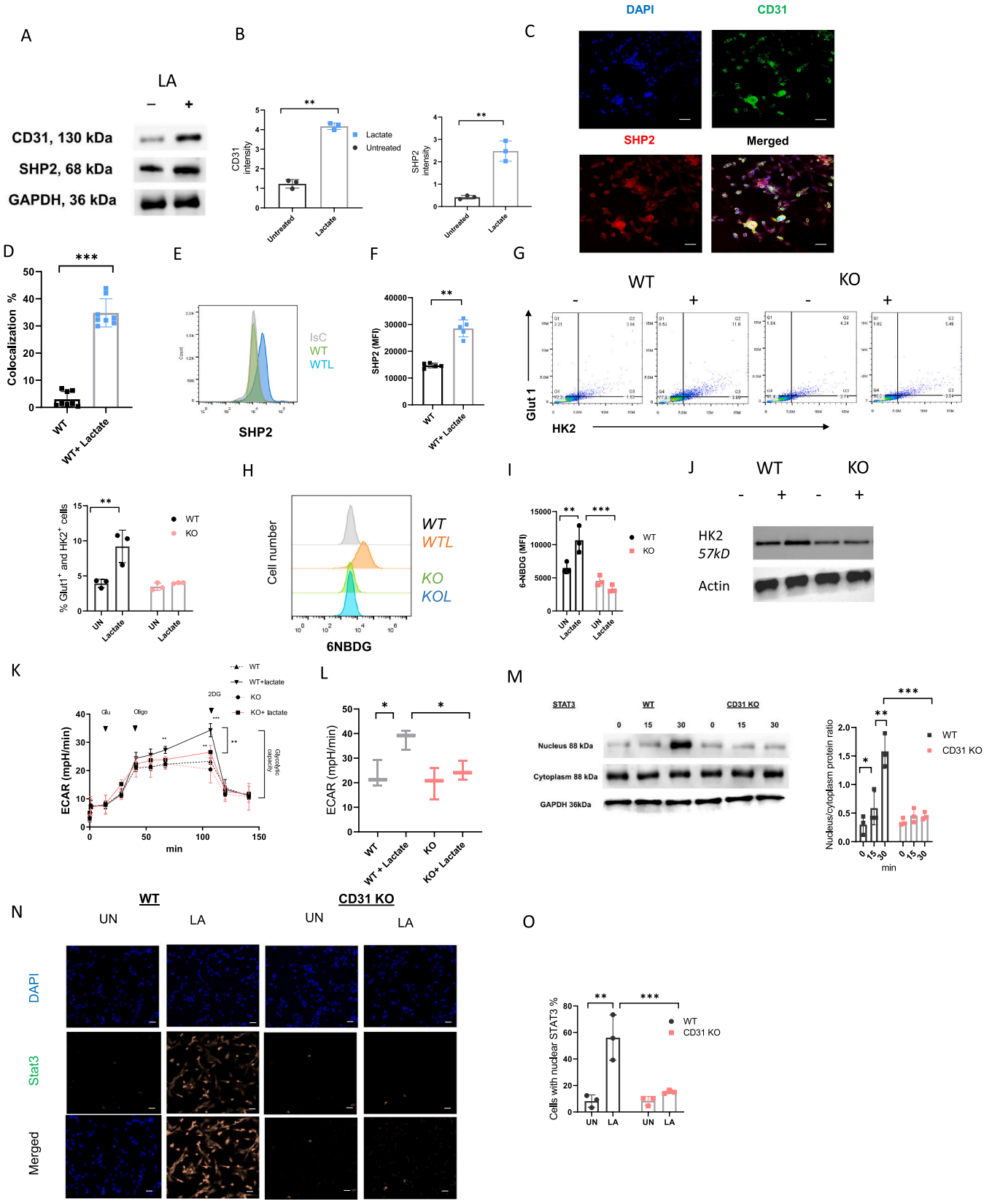
Increasingly recognized as a double-edged sword in autoimmune diseases, CD31 has both inhibitory and potentially detrimental effects. On one hand, CD31 can act as an inhibitory receptor, dampening the transmigrating T-lymphocytes and preventing excessive inflammation [4,8]. On the other hand, some suggest that the promotion of new blood vessel formation in nutrient- or oxygen-deprived regions, such as in hypoxia, can have detrimental consequences, including resistance to therapy, the formation of metastases, and disease progression [9,10]. The precise mechanism by which endothelial CD31 motifs mediate communication signals in synovitis is still not fully understood.

In this study, we demonstrated the presence of LA accumulation in the inflamed joint and observed that CD31 phosphorylation and SHP-2 are upregulated in RA ECs. Stimulation of CD31 by LA led to an increase in the expression of GLUT1, a key glucose transporter, and the key glycolytic enzyme HK2. Our study outcomes reinforce previous findings, showing that increased glycolytic activity along with the involvement of CD31, GLUT1, and SHP2 is instrumental in the regulation of vascular function in metabolic diseases [3]. Interestingly, fibroblast-like synoviocytes (FLS) in RA exhibit increased glycolytic metabolism under metabolic stress [9]. When glucose levels are reduced or glycolytic inhibitors like 2-DG are used, there is a reduction in cytokine secretion, proliferation, and migration of FLS, resulting in a decrease in disease severity in a mouse model of arthritis [11]. Silencing HK2 reduces the tissue invasiveness of RA FLS, while its overexpression leads to increased levels of metalloproteinase (MMP), IL6, and IL8, along with an enhanced migratory rate [12]. Additionally, the HK2 inhibitor, 3-bromopyruvate (BrPA) has been found to modulate the Th17/Treg ratio, suppress dendritic cell activation, and reduce cytokine expression [13].

Recent studies suggest that autophagy may serve as a dynamic mechanism enabling ECs to adjust their bioenergetic and biosynthetic needs in response to the changing environment, presence of angiogenic cues, or intrinsic and extrinsic insults or injuries [14]. We show that in response to LA, CD31 ECs promote crucial pro-autophagic proteins, including pAMPK and key transcription components of the autophagy machinery such as ATG5, BECN1, and LC3. Recent research has shown that autophagy plays a key role in regulating TNF-alpha-mediated joint destruction in experimental arthritis [15]. Moreover, glycolysis and autophagy have been demonstrated to be interconnected through various signaling pathways involving mTOR, HIF, AMPK, PI3K/AKT, and JNK. Besides, HK2 can translocate to the mitochondria, where it triggers an autophagic and anti-apoptotic response by interacting with the voltage-dependent anion channel [16].

We present additional evidence suggesting that CD31 ECs play a role in triggering broader vesicular trafficking processes, such as exocytosis, in response to LA. This is consistent with recent data demonstrating CD31's involvement of in exocytosis [17,18], endocytosis [18], and phagocytosis [19], emphasizing the significance of regulating autophagosome in modulating EC junctions and inflammation [20]. Additionally, our results show that CD31 may play a regulatory role in the activation of STAT3 in the context of RA, as KO of CD31 inhibits the nuclear translocation of STAT3 in ECs treated with LA. Previous research has indicated that STAT3 activation can contribute to the development of chronic arthritis, influencing the abnormal growth and survival characteristics of synovial cells in RA [21,22].

Our findings were complemented by a metabolomic analysis of CD31 ECs in response to LA. Specifically, the levels of succinate were found to be higher in LA-treated CD31 ECs compared to CD31 KO ECs. This aligns with previous research demonstrating an accumulation of succinate in inflammatory macrophages activated by lipopolysaccharides (LPS), likely resulting from changes in the TCA cycle [23]. Furthermore,



(caption on next page)

Fig. 2. CD31 signal contribute to glycolysis EC. (A-B) CD31 WT ECs were exposed to 100 nM LA for45 min followed by immunoblotting with anti-CD31 and anti-SHP2 antibodies. (C) CD31 WT EC were treated with LA for 6 h, and SHP2 localization was assessed by confocal imaging (Scale bars: 50 μm). (D) For quantification, 500 cells per coverslip were analyzed, and the bar graph illustrates the percentage of cells displaying nuclear co-localization mean values ± SD. Statistical analysis was performed using one-way ANOVA with Tukey post-hoc test. (E-F) FACS measurement of SHP2 in CD31 WT ECs treated with LA, ***$p < 0.001$, ****$p < 0.0001$. (G) Glut1 and HK2 expression in CD31 WT/KO ECs. (H-I) Measurement of 6NBDG uptake in CD31 WT/ KO ECs with or without LA treatment for 6 h, quantified by flow cytometry. (J) HK2 expression by western blot analysis. (K) Extracellular acidification rates (ECAR) in CD31 WT/ KO ECs ±LA treatment for 2 h, and consecutively injected with glucose, oligomycin and 2-DG (L) ECAR values (mpH/min) are shown. Mean ± SEM (n = 3 independent experiments). (M) Nuclear fractions were isolated from ECs treated with LA for 0–30 min and subjected to anti-STAT3 immunoblot assay. The bar graph shows protein quantification by densitometry in three independent experiments ± SEM. Statistical analysis was performed using one-way ANOVA with Tukey post-hoc test. (N) ECs were stained with anti-STAT3 (in red) and DAPI (in blue) for confocal analysis. (O) For quantification, 500 cells per coverslip were analyzed, and the bar graph illustrates the percentage of cells displaying nuclear STAT3 localization, measured in three independent experiments ± SD. Scale bar = 50 μm. Statistical analysis was performed using one-way ANOVA with Tukey post-hoc test for CD31 WT/KO±LA, ***$p < 0.001$.

succinate triggers the activation of hypoxia-inducible factor (HIF)-1α and increases the production of pro-inflammatory interleukin (IL)-1β [24]. Another study has demonstrated elevated levels of succinate in the synovial fluid of individuals with RA. This excess succinate has been shown to trigger the release of IL-1β from macrophages in a manner dependent on GPR91. Notably, various drugs used in RA treatment impact metabolic signalling pathways. For instance, antagonists of GPR91 [25] may serve as promising therapeutic molecules for RA treatment, while inhibition of succinate dehydrogenase (SDH) activity limits succinate accumulation and prevents angiogenesis, offering a potential therapeutic strategy to attenuate neo-angiogenesis in arthritis [26].

Furthermore, our findings indicate a decrease in fumarate levels in CD31 ECs treated with LA, aligning with evidence that both fumarate and itaconate possess anti-inflammatory effects [27]. Recent research has demonstrated that the methyl ester dimethyl fumarate (DMF) has received approval for treating relapsing multiple sclerosis. Intriguingly, DMF has been reported to diminish osteoclastogenesis and bone destruction by increasing the expression of nuclear factor erythroid 2–related factor 2 (NRF2)-mediated antioxidant genes while decreasing reactive oxygen species levels [28,29]. Therefore, our study identifies the mechanistic role of CD31 in regulating metabolites, presenting potential avenues for therapeutic intervention.

We have demonstrated that CD31's ITIM (Immunoreceptor Tyrosine-based Inhibitory Motif) domains at Y663 and Y686 in the C-terminus mediate ligand-receptor interactions on ECs, thereby influencing cellular signaling [3,4]. Our current findings indicate that substituting amino acids Y663F and Y686F in CD31, or KO, leads to an increase in oxidative phosphorylation and a decrease in HK2. In addition, our data demonstrates that CD31 with Y663F and Y686F mutations, when treated with LA, exhibit the inhibition of key transcription factors involved in inflammation, particularly STAT3, in comparison to the WT CD31. This underscores a potential therapeutic target in manipulating the C-terminus of the CD31 motifs.

In line with our data, certain drugs used in the treatment of RA affect metabolic signaling pathways. For example, in the presence of tofacitinib, there was a significant enhancement of oxidative phosphorylation and mitochondrial respiration in RA FLS, coupled with a reduction in glycolysis and key glycolytic enzymes including HK2, glycogen synthase kinase 3α (GSK-3α), lactate dehydrogenase A, and HIF-1α in both RA FLS and synovial explants [30]. Another study has shown that mTOR can be a potential therapeutic target for suppressing abnormal T cell differentiation during the early stages of RA [31].

Altogether, the evidence we provide supports the role of CD31 signal activation in triggering a metabolic shift in autophagy processes. This shift is necessary to meet the increased demands for energy and biomolecules required for vasculature of the synovium in RA. Thus, our findings contribute to understanding endothelial metabolic adaptation in RA, and the regulation of metabolic reprogramming by CD31 may offer novel targets for the prevention and therapy of diseases.

4. Material and methods

4.1. Experimental Section

4.1.1. Animal experiments

All the animal experiments were reviewed and approved by the ethics committee of Hong Kong Baptist University REC/20–21/0584). All animal experiments conducted in this study were complied with the WMA Statement on animal use in biomedical research. To establish the CIA model. On day 0, mice were immunized intradermally at the base of the tail with 150 μg of chicken CII (Sigma) emulsified with an equal volume of Freund's complete adjuvant containing 200 μg of H37Ra Mycobacterium tuberculosis (BD Biosciences, cat. no. 231141). On day 21, mice were given a booster intradermal injection of 150 μg of chicken CII in Freund's incomplete adjuvant (Difco).

4.1.2. Clinical materials and tissue preparation

The human studies were all approved by the Ethics Committee of Shanghai Sixth People's Hospital in accordance with the World Medical Association's Declaration of Helsinki and gave written informed consent for this study. RA patients met the 2010 American College of Rheumatology (ACR) classification criteria [33].

Human cohort 1: All the patients were divided into two groups, including the healthy people (n=22 for 22–37 years old) and RA (n=27 for 18–44 years old). The tubes were left for 20 min to allow for clotting and centrifuged at 15,609 × *g* for 10 min, at 4 °C. Serum was stored at −80 °C until analysis. Lactate in serum was detected using human lactate ELISA kit (ab287808).

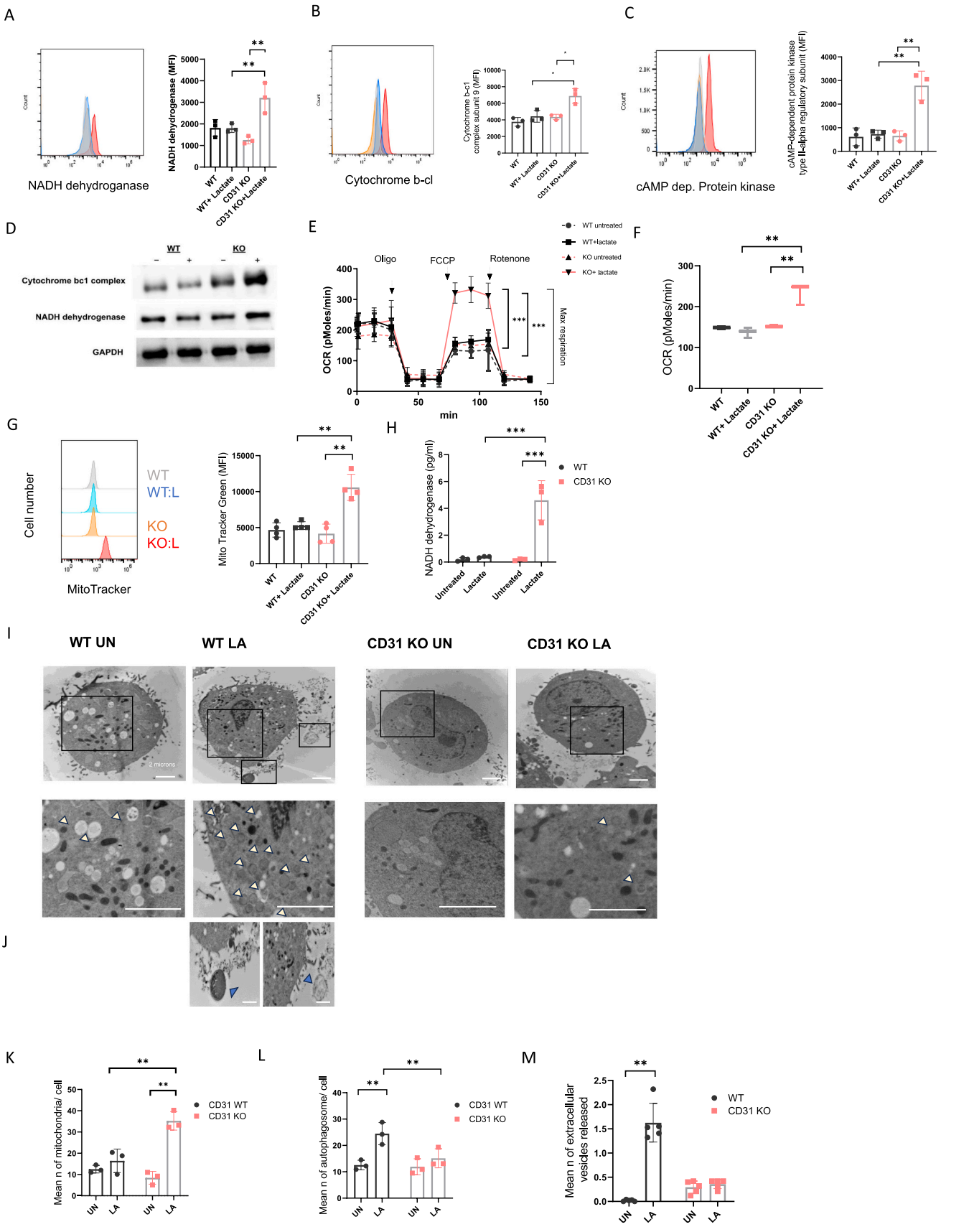
Human cohort 2: We collected human synovium extracted from patients with RA or OA undergoing total joint replacement at the Shanghai Sixth People's Hospital. OA (n = 6) and RA (n = 5) were included in our study.

4.1.3. Electron microscopy of resin-embedded cells

For high-pressure freezing suspension, cultured endothelial cells were harvested by filtering and immediately frozen in a high-pressure freezing apparatus (HPF010; Bal-Tec, Balzers, Liechtenstein). For subsequent freeze substitution, the material was kept at −85 °C for 60 h before slowly being warmed to 0 °C for a period of 18 h. Substitution was performed in an AFS freeze substitution unit (Leica, Bensheim, Germany). The sections were poststained with aqueous uranyl acetate/lead citrate, and images were captured with a Hitachi H7650 transmission electron microscope (Hitachi High-Technologies) operating at 80 kV.

4.1.4. Isolation and culture of primary microvascular endothelial cells

Endothelial cells (ECs) were isolated from synovial tissues of C57BL/6 mice following a previously published protocol [32] and cultured in (DMEM ThermoFisher 41966), supplemented with 10 % FCS). When confluent, cells were detached with trypsin/EDTA (Gibco, T4049) and passaged. Cells were used for up to 4 passages in culture.



(caption on next page)

Fig. 3. Specific deletion of CD31 in EC triggered mitochondrial respiration upon LA stimulation. (A-C) Intracellular staining of NADH2 dehydrogenase, cytochrome bc1 complex, and cAMP-dependent protein kinase in CD31 WT/KO:LA was measured by flow cytometry. (D) Western blotting analysis of the cytochrome bc1 complex, and NADH1 dehydrogenase expression in WT/KO EC:LA. GAPDH was used as a loading control. (E-F) The oxygen consumption rate (OCR) of WT/KO EC ±LA was measured by a Seahorse flux analyzer. Dot lines indicate the time and period of glucose, oligomycin (Oligo) (1 μM), carbonyl cyanide-p- trifluoromethoxy phenylhydrazone (FCCP) (1 μM), rotenone (ROT), or antimycin (Ant) (1 μM) being added during Seahorse experiments. Maximal respiration was calculated (n = 3 biological replicates). Statistical tests were two-sided. (G) Mito Tracker® staining of CD31 WT/KO ECs treated with LA was evaluated by flow cytometry. (H) The expression of NADH dehydrogenase significantly increased in response to LA in CD31 KO EC, as measured after 6 h by ELISA. The data shown are the MFI value ± SD of three independent experiments. (I-J) Mitochondrial number, autophagosome, and extracellular vesicles released by CD31/KO±LA ECs (4 hr) were identified by transmission electron microscopy (TEM) (I) TEM revealed an increase in the number of mitochondria, autophagosomes, and vesicle release. (J) The size of the vesicles ranged from approximately 50–150 nm, consistent with extracellular vesicles (EVs). White arrows indicate EVs released by ECs. Scale bar = 500 nm, representing three independent experiments. (K-M) Bar charts show the average changes and statistical analysis between each group. (R-S). The data represents the mean value (±SD) of three independent experiments. **p < 0.01, ***p <0.001, ****p <0.0001.

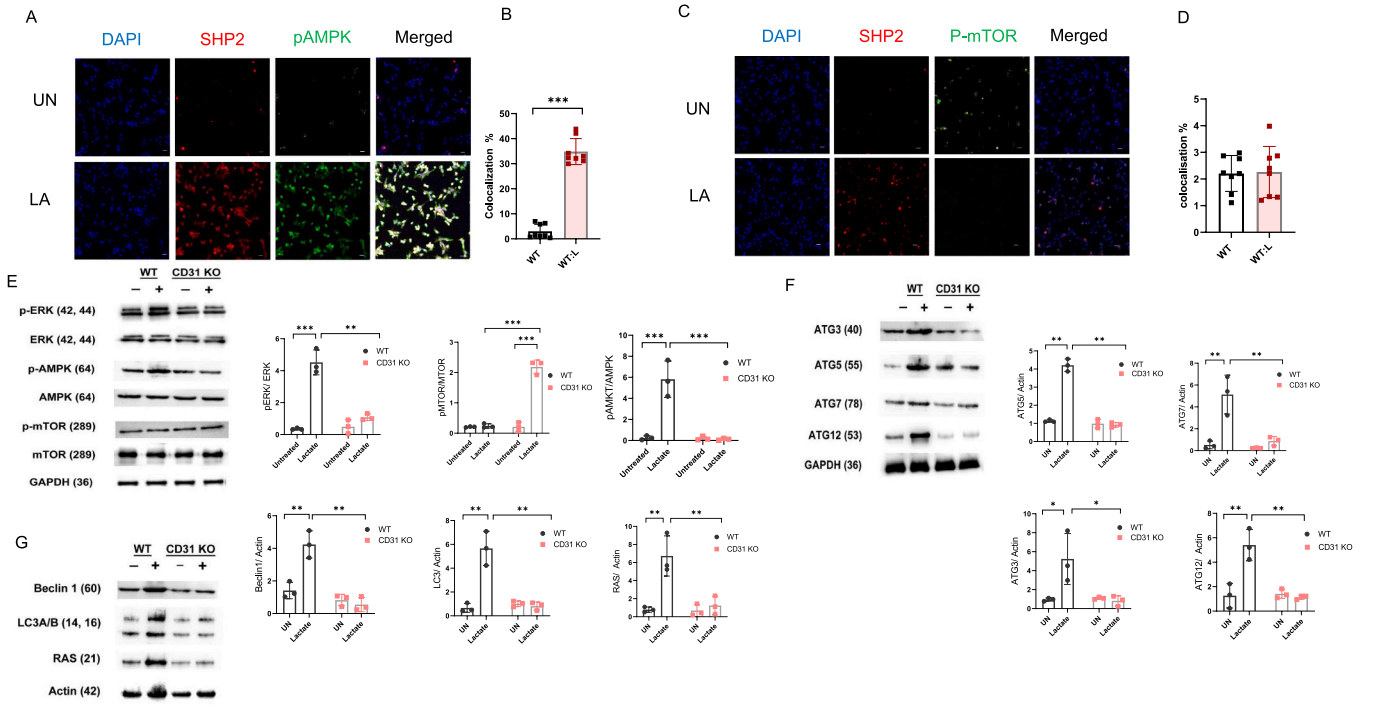


Fig. 4. CD31 signals enhanced autophagy in response to LA stimulation. (A-B) Immunofluorescence was performed using antibodies against SHP2 and p-AMPK in WT and KO ECs treated with LA for 4 hours. (C-D) Immunofluorescence staining for SHP2 and p-mTOR in WT and CD31-KO ECs treated with LA for 4 h. For quantification, 500 cells per coverslip were analyzed, and the bar graph shows the percentage of cells displaying co-localization measured ± SD. Scale bar = 50 μm. (E-G) Representative and summarized western blotting data demonstrating increased expression of phosphorylated AMPK, and autophagy proteins, while a decrease in p-mTOR in WT ECs treated with LA for 4 h. Statistical analysis was performed using the nonparametric Mann-Whitney test. CD31 WT/KO±LA. ***p < 0.001.

4.2. Immunohistochemistry

Deparaffinized synovial tissue sections in each group were subjected to Ag retrieval in citrate buffer solution (0.01 M), and then blocked by endogenous peroxidase blocking solution for 15 min. After that, the sections were probed with the required primary antibodies, including Recombinant Anti-Beclin 1 antibody [EPR19662] (ab207612); rabbit monoclonal anti-CD31^{+} (EPR17259, ab182981, Abcam), a rabbit monoclonal anti-HK2 (c35c4, 2024 S, Cell signaling), a rabbit monoclonal anti-Glut1 (E4S6I, 73015 S, Cell signaling). The fluorophore-conjugated secondary antibodies used was a goat anti-rabbit IgG H&L (HRP, ab205718, Abcam). The data were analyzed by Tissue FAXS-S Plus system (tissue Gnostics, Austria).

4.3. Quantitative real-time polymerase-chain reaction (qRT-PCR)

Expression was calculated using the ΔΔct method and normalized to a housekeeper gene (GAPDH). Primers for qPCR were designed with the help of online tools (Primer 3Plus) using at least one exon junction-binding site per primer pair.

HK2	GAGTTTGACCTGGATGTGGTTGC	CCTCCATGTAGCAGGCATTGCT
ATG7	CGTTGCCCACAGCATCATCTTC	CACTGAGGTTCACCATCCTTGG
ATG5	ATGTGCTTCGAGTGTGTGG	AATGCCATTCAGTGGTGTG
Beclin−1	CTGGACACTCAGCTCAACGTCA	CTCTAGTGCCAGCTCCTTTAGC
LC3B	GAGAAGCAGCTTCCTGTTCTGG	GTGTCCGTTCACCAACAGGAAG
GAPDH	GTCTCCTCTGACTTCAACAGCG	ACCACCCTGTTGCTGTAGCCAA

4.4. Cellular fractionation and isolation of nuclei

ECs (5–10 × 10^{6}) were cultured in 60-mm diameter culture dishes until ~80 % confluency. For isolation of nuclear extracts, the cells were then collected into microtubes, centrifuged, and resuspended in 200 μL of 10.0 mM Hepes (Gibco, 15630080), pH 7.9, containing 10.0 mM KCl, 1.5 mM $MgCl_2$, and 0.5 mM dithiothreitol. After incubation at 4 °C for 15 min, the cells were lysed by passing them through a 22-gauge needle. Next, the cells were centrifuged and the supernatant containing the cytoplasmic fraction was collected and frozen in small aliquots. The pellet, which contained the nuclei, was resuspended in 150 μL of 20 mM Hepes, pH 7.9, containing 20 % v/v glycerol, 0.1 mM KCl, 0.2 mM EDTA

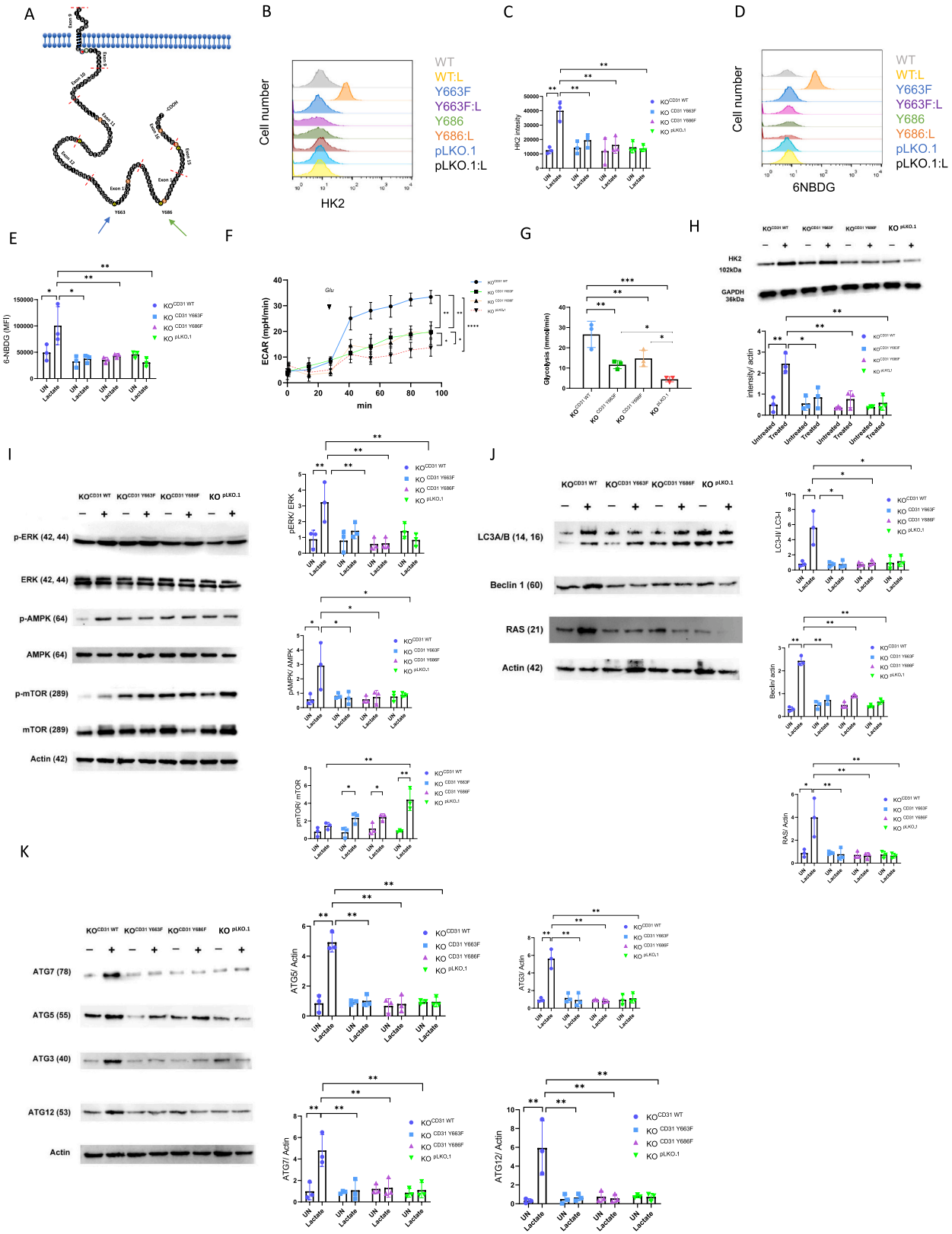
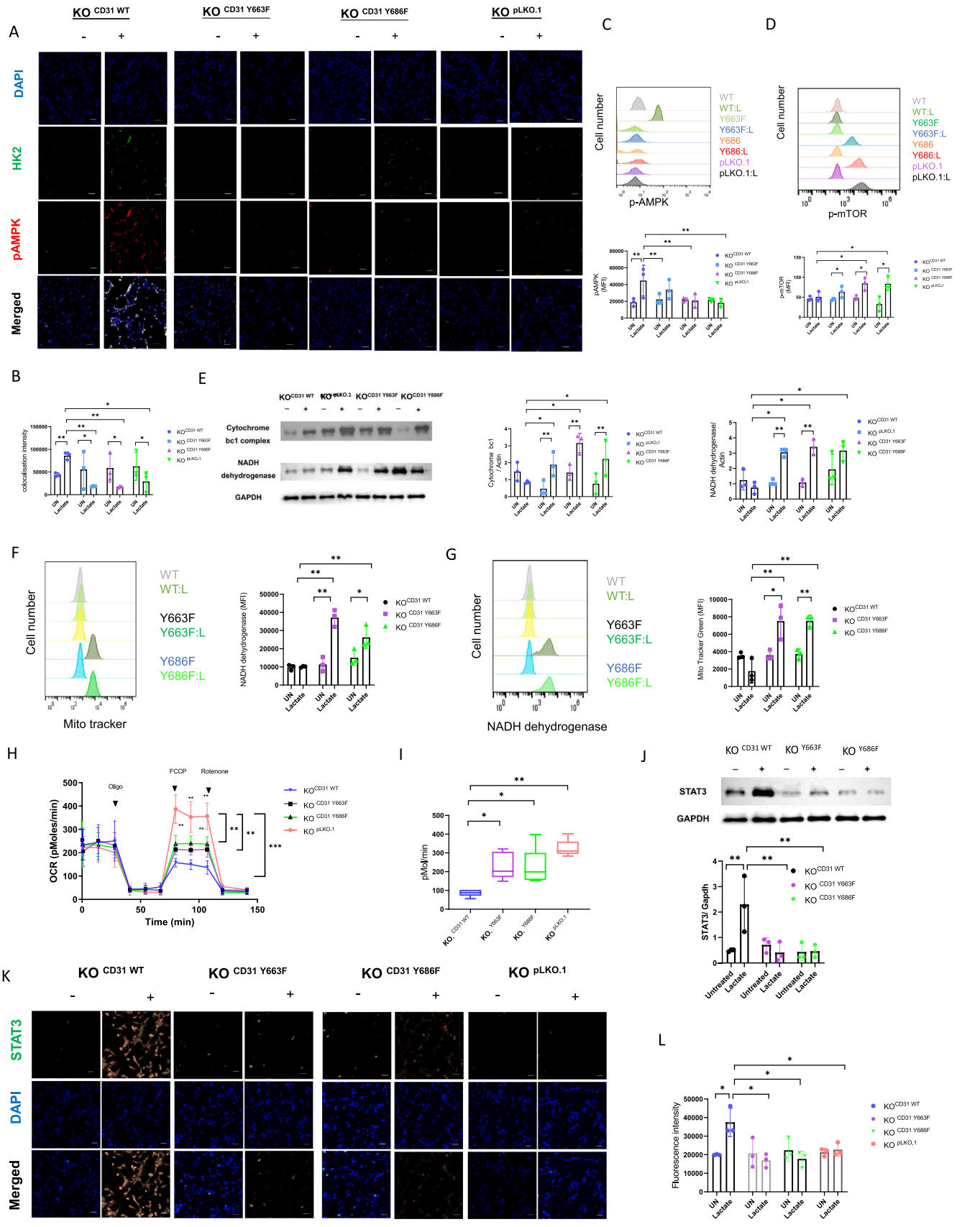


Fig. 5. CD31 Y663F and Y686F EC suppressed autophagy and glycolysis. (A) CD31 gene constructs with mutations leading to the loss-of-function amino acid substitutions Y663F and Y686F in the ITIMs were generated and expressed by lentiviral transduction into CD31KO ECs (CD31Y663F and CD31Y686F). As a control, CD31KO ECs were transduced with a WT CD31 gene construct or an empty plasmid (pLKO.1, mock). (B-C) Measurement of HK2 expression by FACs in ECs treated with LA. (D-E) Representative FACs analysis of 6NBDG uptake and quantification. (F-G) ECAR analysis of ECs treated with LA. The bar chart represents glycolysis value (*$p < 0.05$, **$p < 0.01$, ***$p < 0.001$). (H) HK2 from ECs treated with LA was analyzed by Western blot. (I) p-ERK, p-AMPK, and p-mTOR. (J) LC3A, Beclin, RAS. (K) ATG 5,7,3 and 12 expression in mock-, WT-, CD31Y663F-, and CD31Y686F-transduced CD31KO ECs exposed to 100 nM LA for 6 h as measured by western blot (n = 3 independent experiments). (Right) Results are given as means ± SEM. Student's t test.



(caption on next page)

Fig. 6. CD31^{Y663F} and ^{Y686F} EC expression suppressed AMPK phosphorylation and HK2 activation in EC with LA. (A-B) Intracellular staining of p-AMPK (red) and HK2 (green) in stimulated ECs (Mock-, WT-, CD31Y663F-, and CD31Y686F-transduced CD31KO) ±LA for 4 hr. Results show mean + SEM of three independent experiments. *p < 0.05, **p < 0.01. (C-D) The MFI of pAMPK and p-MTOR were measured in three independent experiments, respectively. Data are mean ± SD. One-way Anova with Tuckey post-hoc test. *p < 0.05, **p < 0.01. (E) Western blot analysis shows protein expression of cytochrome bc1 complex and NADH dehydrogenase in mock-, WT-, CD31Y663F-, and CD31Y686F-transduced CD31KO ECs treated with 100 nM LA for 6 h. (F) Increased MitoTracker in mutants as detected by FACS analysis. Data are represented as MFI ± SEM. (G) FACs analysis shows increased NADH dehydrogenase expression in mutants generated ECs treated with LA. Bar chart shows the increase in protein level observed in mutants and CD31KO treated with LA. (H-I) OCR measured by Seahorse analysis showed that treatment with mutants significantly enhanced the OCR in mutants when compared to WT treated with LA. Results are given as means ± SEM. The CD31 Y663F and Y686F mutations inhibit mitochondrial accumulation and STAT 3 activation in response to LA treatment in ECs. (J) Nuclear fractions were isolated from mock and mutants and subjected to anti-STAT3 immunoblot assay for 4 hr. HD is a tag control. The bar graph shows protein quantification by densitometry in three independent experiments ± SEM. (K-L) Representative confocal images measuring STAT3 (red), and quantification was significantly increased in CD31 Y663F and Y686F ECs treated with LA. Scale bar = 50 μm. For quantification, 500 cells per coverslip were analyzed. One-way Anova with Tuckey post-hoc test. *p < 0.05, **p < 0.01.

(Invitrogen, AM9912), 0.5 mM dithiothreitol (Thermo Scientific, A39255), and 0.5 mM phenylmethanesulfonyl fluoride (Sigma Aldrich,10837091001) and then stirred at 4 °C for 30 min. The nuclear extracts were then centrifuged (25 min, 14000 g) at 4 °C in a microcentrifuge. The supernatant was collected, aliquoted into small volumes, and stored at −80 °C.

4.5. Coimmunoprecipitation

ECs (10^7) were lysed in 1 mL lysis buffer [20 mM Tris·HCl (pH 8), 1 % Triton X-100, 150 mM NaCl, 1 mM Na_3VO_4, 1 mM 4-benzenesulfonyl fluoride hydrochloride, 1 μg/mL leupeptin]. After centrifugation, the lysate was precleared using Protein G-Sepharose (Sigma-Aldrich, P3296) for 30 min at 4 °C and then was incubated with specific antibodies for 1 h before the addition of Protein G-Sepharose and overnight incubation at 4 °C. Samples then were washed three times with lysis buffer, boiled in SDS/PAGE sample buffer, resolved using 10 % SDS/PAGE, and analyzed by Western blotting.

4.6. Immunoprecipitation-mass spectrometry (IP-MS)

Proteins were extracted from EC treated ± 100 nM LA before applying to SDS-PAGE gel electrophoresis. The gel was then stained with Imperial™ Protein Stain (Pierce) after SDS–PAGE separation, and proteins were cut out for in-gel trypsin digestion. The mixed IP sample was fractionated by nano-liquid chromatography-MS (nano-LCMS) using an UltiMate 3000 RSLCnano system (Thermo Fisher Scientific). MS data were then acquired with an Orbitrap Fusion Lumus mass spectrometer (Thermo Fisher Scientific). Proteins with matched high confident peptides were retained and shown in Datasets.

4.7. Measurement of ECAR and OCR

Real time bioenergetics analysis of extracellular acidification rates (ECAR) and oxygen consumption rates (OCR) of ECs was performed using the XF analyzer (Seahorse Biosciences). ECs were cultured in serum free, unbuffered XF assay medium (Seahorse biosciences, Cat 102365–100) for 1 h. The cells were then seeded (6×10^5/well) into the seahorse XF24 cell plates for analysis. Perturbation profiling of the use of metabolic pathways by ECs was achieved by the addition of oligomycin (1 μM), FCCP (1 μM), Antimycin A (1 μM), rotenone (1 μM), D-glucose (10 mM), 2-deoxy-D-glucose (2DG, 50 mM; all from Seahorse biosciences, Cat# 103020–100 and 103015–100). Experiments with the Seahorse system were done with the following assay conditions: 2 min mixture; 2 min wait; and 4–5 min measurement. Metabolic parameters were calculated by Wave v2.4.1 Software. Experiments were done in at least triplicate wells.

4.8. Flow cytometry

Cells were harvested and suspended in FACS buffer (PBS, 1 % BSA, 0.01 % sodium azide), fixed using fixation buffer (PBS, 4 % paraformaldehyde, 1 % FCS). Then, cells were stained with the appropriate concentration of fluorescence-conjugated antibodies, or isotype control antibodies, according to the manufacturer's instructions. Mean Fluorescence Intensity (MFI) was measured by a FACSAria cell sorter (Becton Dickinson). For *in-vitro* 6NBDG uptake assay, freshly isolated EC were washed in PBS and resuspended in glucose-free cell medium (Gibco, Cat11879–020). 6-NBDG (Life Technologies, CatN23106) was then added to the medium and cells were incubated for 15 min at 37° C. Finally, the cells were washed twice with PBS, suspended in flow cytometry buffer and MFI was analyzed by flow cytometry. Acquired samples were analyzed using FlowJo 7.6 software (Tree Star, Inc.).

4.9. Gene ontology enrichment and network analysis

Gene Ontology (GO) enrichment and network analysis were performed by using ClueGO function in CytoScape v3.8.0 [12,13]. GO describes biological process, molecular function, and cellular component for genes. Only "cellular component" was selected for the enrichment analysis in Datasets S2. P-value was calculated by two side hypergeometric test, and its False Discovery Rate was adjusted by Bonferroni–Holm method. Term-term interactions and GO clusters were inferred by Kappa score [34].

4.10. Metabolomic array

10^7 WT/CD31 KO ECs ± 100 nM LA were collected and homogenized with a mixture of Millipore ultrapure water and cold methanol. After centrifugation at 13500 g and 4 °C for 10 min, a 30 μL aliquot of the supernatant was carefully transferred to a 96 well plate for derivatization. The plate was then transferred to a Biomek 4000 workstation (Biomek 4000, Beckman Coulter, Inc., Brea, California, USA). 20 μL of freshly prepared derivative reagents (200 mM 3-NPH in 75 % aqueous methanol and 96 mM EDC-6 % pyridine solution in methanol) was added to each well. The plate was sealed, and the derivatization was carried out at 30°C for 60 min. After derivatization, the plate was lyophilized (Labconco, Kansas City, MO, USA) to dry. Then 400 μL of ice-cold 50 % methanol solution was added to resolve the sample, followed by 4000 g centrifugation at 4°C for 30 min. 135 μL of supernatant was transferred to a new 96-well plate in each well. Finally, the plate was sealed for LC-MS analysis. The raw data files generated by UPLC-TQXMS were processed using the TMBQ software (v1.0, HMI, Shenzhen, Guangdong, China) to perform peak integration, calibration, and quantification for each metabolite.

Statistical analysis

Clinical scores were analyzed with the nonparametric Mann–Whitney U test. Cytokine and collagen-specific IgG levels were compared with a Student's test

CRediT authorship contribution statement

Aiping Lu: Supervision. **Kenneth Chat Pan Cheung:** Writing – review & editing, Writing – original draft, Supervision, Resources, Project

administration, Methodology, Investigation, Funding acquisition, Formal analysis, Data curation, Conceptualization. **Wei Jia:** Supervision. **Xiaojiao Zheng:** Methodology, Supervision. **Xingxuan Chen:** Data curation. **Silvia Fanti:** Formal analysis. **Jiao Ma:** Conceptualization. **Lu Wang:** Methodology. **Fabien Gosselet:** Conceptualization. **Hao Shen:** Methodology. **Mingzhang Li:** Conceptualization. **Loiola Rodrigo Azevedo:** Formal analysis.

Declaration of Competing Interest

The authors declare that they have no known competing financial interests or personal relationships that could have appeared to influence the work reported in this article

Data Availability

Confidential

Appendix A. Supporting information

Supplementary data associated with this article can be found in the online version at doi:10.1016/j.phrs.2024.107346.

References

[1] N.A. Cummings, G.L. Nordby, Measurement of synovial fluid pH in normal and arthritic knees, Arthritis Rheum. 9 (1) (1966) 47–56.
[2] W.A. Muller, Leukocyte-endothelial-cell interactions in leukocyte transmigration and the inflammatory response, Trends Immunol. 24 (6) (2003) 327–334.
[3] K.C.P. Cheung, S. Fanti, C. Mauro, G. Wang, A.S. Nair, H. Fu, et al., Preservation of microvascular barrier function requires CD31 receptor-induced metabolic reprogramming, Nat. Commun. 11 (1) (2020) 3595.
[4] K. Cheung, L. Ma, G. Wang, D. Coe, R. Ferro, M. Falasca, et al., CD31 signals confer immune privilege to the vascular endothelium, Proc. Natl. Acad. Sci. USA 112 (43) (2015) E5815–E5824.
[5] M.B. Schaaf, D. Houbaert, O. Mece, P. Agostinis, Autophagy in endothelial cells and tumor angiogenesis, Cell Death Differ. 26 (4) (2019) 665–679.
[6] B. Cruys, B.W. Wong, A. Kuchnio, D. Verdegem, A.R. Cantelmo, L.C. Conradi, et al., Glycolytic regulation of cell rearrangement in angiogenesis, Nat. Commun. 7 (2016) 12240.
[7] F. Humby, M. Lewis, N. Ramamoorthi, J.A. Hackney, M.R. Barnes, M. Bombardieri, et al., Synovial cellular and molecular signatures stratify clinical response to csDMARD therapy and predict radiographic progression in early rheumatoid arthritis patients, Ann. Rheum. Dis. 78 (6) (2019) 761–772.
[8] L. Ma, K.C. Cheung, M. Kishore, S. Nourshargh, C. Mauro, F.M. Marelli-Berg, CD31 exhibits multiple roles in regulating T lymphocyte trafficking in vivo, J. Immunol. 189 (8) (2012) 4104–4111.
[9] H.C. Sullivan, M.A. Edgar, C. Cohen, C.K. Kovach, K. HooKim, M.D. Reid, The utility of ERG, CD31 and CD34 in the cytological diagnosis of angiosarcoma: an analysis of 25 cases, J. Clin. Pathol. 68 (1) (2015) 44–50.
[10] V. Venkataramani, S. Kuffer, K.C.P. Cheung, X. Jiang, L. Trumper, G.G. Wulf, et al., CD31 expression determines redox status and chemoresistance in human angiosarcomas, Clin. Cancer Res. Off. J. Am. Assoc. Cancer Res. 24 (2) (2018) 460–473.
[11] R. Garcia-Carbonell, A.S. Divakaruni, A. Lodi, I. Vicente-Suarez, A. Saha, H. Cheroutre, et al., Critical role of glucose metabolism in rheumatoid arthritis fibroblast-like synoviocytes, Arthritis Rheumatol. 68 (7) (2016) 1614–1626.
[12] M.F. Bustamante, P.G. Oliveira, R. Garcia-Carbonell, A.P. Croft, J.M. Smith, R. L. Serrano, et al., Hexokinase 2 as a novel selective metabolic target for rheumatoid arthritis, Ann. Rheum. Dis. 77 (11) (2018) 1636–1643.
[13] T. Okano, J. Saegusa, K. Nishimura, S. Takahashi, S. Sendo, Y. Ueda, et al., 3-bromopyruvate ameliorate autoimmune arthritis by modulating Th17/Treg cell differentiation and suppressing dendritic cell activation, Sci. Rep. 7 (2017) 42412.
[14] C.K. Domigan, C.M. Warren, V. Antanesian, K. Happel, S. Ziyad, S. Lee, et al., Autocrine VEGF maintains endothelial survival through regulation of metabolism and autophagy, J. Cell Sci. 128 (12) (2015) 2236–2248.
[15] N.Y. Lin, C. Beyer, A. Giessl, T. Kireva, C. Scholtysek, S. Uderhardt, et al., Autophagy regulates TNFalpha-mediated joint destruction in experimental arthritis, Ann. Rheum. Dis. 72 (5) (2013) 761–768.
[16] V.P. Tan, S. Miyamoto, HK2/hexokinase-II integrates glycolysis and autophagy to confer cellular protection, Autophagy 11 (6) (2015) 963–964.
[17] E.M. Buckingham, K.W. Jarosinski, W. Jackson, J.E. Carpenter, C. Grose, Exocytosis of Varicella-Zoster virus virions involves a convergence of endosomal and autophagy pathways, J. Virol. 90 (19) (2016) 8673–8685.
[18] S.A. Tooze, A. Abada, Z. Elazar, Endocytosis and autophagy: exploitation or cooperation? Cold Spring Harb. Perspect. Biol. 6 (5) (2014) a018358.
[19] B.L. Heckmann, E. Boada-Romero, L.D. Cunha, J. Magne, D.R. Green, LC3-associated phagocytosis and inflammation, J. Mol. Biol. 429 (23) (2017) 3561–3576.
[20] N. Reglero-Real, L. Perez-Gutierrez, A. Yoshimura, L. Rolas, J. Garrido-Mesa, A. Barkaway, et al., Autophagy modulates endothelial junctions to restrain neutrophil diapedesis during inflammation, Immunity 54 (9) (2021) 1989–2004, e9.
[21] F. Wang, T.K. Sengupta, Z. Zhong, L.B. Ivashkiv, Regulation of the balance of cytokine production and the signal transducer and activator of transcription (STAT) transcription factor activity by cytokines and inflammatory synovial fluids, J. Exp. Med. 182 (6) (1995) 1825–1831.
[22] S.Y. Lee, S.K. Kwok, H.J. Son, J.G. Ryu, E.K. Kim, H.J. Oh, et al., IL-17-mediated Bcl-2 expression regulates survival of fibroblast-like synoviocytes in rheumatoid arthritis through STAT3 activation, Arthritis Res. Ther. 15 (1) (2013) R31.
[23] A.K. Jha, S.C. Huang, A. Sergushichev, V. Lampropoulou, Y. Ivanova, E. Loginicheva, et al., Network integration of parallel metabolic and transcriptional data reveals metabolic modules that regulate macrophage polarization, Immunity 42 (3) (2015) 419–430.
[24] G.M. Tannahill, A.M. Curtis, J. Adamik, E.M. Palsson-McDermott, A.F. McGettrick, G. Goel, et al., Succinate is an inflammatory signal that induces IL-1beta through HIF-1alpha. Nature 496 (7444) (2013) 238–242.
[25] A. Littlewood-Evans, S. Sarret, V. Apfel, P. Loesle, J. Dawson, J. Zhang, et al., GPR91 senses extracellular succinate released from inflammatory macrophages and exacerbates rheumatoid arthritis, J. Exp. Med. 213 (9) (2016) 1655–1662.
[26] Y. Li, Y. Liu, C. Wang, W.R. Xia, J.Y. Zheng, J. Yang, et al., Succinate induces synovial angiogenesis in rheumatoid arthritis through metabolic remodeling and HIF-1alpha/VEGF axis, Free Radic. Biol. Med. 126 (2018) 1–14.
[27] E.L. Mills, D.G. Ryan, H.A. Prag, D. Dikovskaya, D. Menon, Z. Zaslona, et al., Itaconate is an anti-inflammatory metabolite that activates Nrf2 via alkylation of KEAP1, Nature 556 (7699) (2018) 113–117.
[28] R.J. Fox, D.H. Miller, J.T. Phillips, M. Hutchinson, E. Havrdova, M. Kita, et al., Placebo-controlled phase 3 study of oral BG-12 or glatiramer in multiple sclerosis, N. Engl. J. Med. 367 (12) (2012) 1087–1097.
[29] Y. Yamaguchi, H. Kanzaki, Y. Katsumata, K. Itohiya, S. Fukaya, Y. Miyamoto, et al., Dimethyl fumarate inhibits osteoclasts via attenuation of reactive oxygen species signalling by augmented antioxidation, J. Cell. Mol. Med. 22 (2) (2018) 1138–1147.
[30] T. McGarry, C. Orr, S. Wade, M. Biniecka, S. Wade, L. Gallagher, et al., JAK/STAT blockade alters synovial bioenergetics, mitochondrial function, and proinflammatory mediators in rheumatoid arthritis, Arthritis Rheumatol. 70 (12) (2018) 1959–1970.
[31] A. Perl, Activation of mTOR (mechanistic target of rapamycin) in rheumatic diseases, Nat. Rev. Rheumatol. 12 (3) (2016) 169–182.
[32] G.S. Duncan, D.P. Andrew, H. Takimoto, S.A. Kaufman, H. Yoshida, J. Spellberg, et al., Genetic evidence for functional redundancy of Platelet/Endothelial cell adhesion molecule-1 (PECAM-1): CD31-deficient mice reveal PECAM-1-dependent and PECAM-1-independent functions, J. Immunol. 162 (5) (1999) 3022–3030.
[33] D. Aletaha, T. Neogi, A.J. Silman, J. Funovits, D.T. Felson, C.O. Bingham, 3rd, et al., 2010 rheumatoid arthritis classification criteria: an American College of Rheumatology/European league against rheumatism collaborative initiative, Ann. Rheum. Dis. 69 (9) (2010) 1580–1588.
[34] G. Bindea, B. Mlecnik, H. Hackl, P. Charoentong, M. Tosolini, A. Kirilovsky, et al., ClueGO: a Cytoscape plug-in to decipher functionally grouped gene ontology and pathway annotation networks, Bioinformatics 25 (8) (2009) 1091–1093.